TRANSITION MEASUREMENT AND ANALYSIS ON A SWEPT WING IN HIGH LIFT CONFIGURATION

A. Séraudie, J. Perraud, F. Moens (*)
ONERA – Centre de Toulouse, (*) : ONERA - Châtillon

Keywords : *laminar-turbulent transition, relaminarisation, high lift system, EUROLIFT*

Abstract

In the framework of the European Research Program EUROLIFT (European High Lift), the ONERA experimental contribution is a basic experiment to study the transition phenomena on an existing swept profile equipped with a slat and a flap in high lift configuration.
In preparation for the tests, the 3D high lift configuration has been computed at ONERA with a Navier Stokes code to get pressure distributions on the different elements.
Preliminary transition prediction work was performed by different EUROLIFT partners (FOI, DASA and ONERA), taking into account leading edge contamination and using the simplified database method.
The tests have been performed in the F1 ONERA low speed pressurised wind tunnel at various sweep angles and Reynolds numbers.
The existing model well equipped in pressure taps was completed by devices to determine the transition location (infrared and hot films).
The tests results have been analysed and the transition determined for all the elements, tested in the different configurations. Moreover we tried to analyse the transition behaviour under the Reynolds number influence in order to illustrate the different transition mechanisms found on this high lift generic model.

1 Introduction

In the framework of the European Research Program EUROLIFT, several series of wind tunnel tests have been planned in order to analyse high lift aerodynamics in a wide range of model complexity and Reynolds numbers. The first experiment, conducted by ONERA, is a basic experiment dedicated to the study of the transition phenomena on an existing swept profile equipped with a slat and a flap. Such experiment should provide a better knowledge of the transition state in a simple high lift configuration which will be used to improve and calibrate the transition prediction tools.
After a description of the different devices used to determine the transition location, this paper will analyse the behaviour of the transition location evolution with Reynolds number, incidence and sweep angles. We will then try to summarise and illustrate the different transition mechanisms found on this high lift generic model : leading edge contamination (L.E. contamination), transition in a separation bubble, relaminarisation and usual 'natural' transition under streamwise instabilities (TS waves) and crossflow instabilities (CF waves).

2 Experimental set-up

The tests have been performed in the F1 ONERA low speed pressurised wind tunnel located at the ONERA center of 'Le Fauga Mauzac', at the end of year 2000 [1]. The swept wing model is a generic high lift model (named AFV for 'Aile à Flèche Variable') tested at various sweep angles and Reynolds numbers (fig. 1). The reference 2D shape of the wing is the RA16SC1 profile. It is a constant chord (0.5m normal chord) swept wing metallic model and the different elements are connected with tracks (slat chord 0.12 m, flap chord 0.145 m).
The metallic AFV model is equipped with 8 rows of 93 pressure taps each (total = 744) distributed over the 3 elements. A wall balance measured forces and moments during the tests. Transition detection was performed using

infrared thermography and 24 hot films distributed along a chordwise section of the 3 elements.
A region of the slat upper side was covered with a thin layer of black paint (see fig. 1) to get a large enough emissivity coefficient. For the tests the infrared camera was installed just behind the right vertical wall of the test section. The camera was placed into a cavity connected to atmospheric conditions as it is not designed to support pressurisation.
To get a good contrast on the infrared images a thermal shift (2 or 3 degrees) was imposed to the flow during the data acquisitions. A determination of the transition location was done, directly by measuring the extent of the clear laminar region close to the leading edge ; this location generally corresponds to the middle of the transition region.

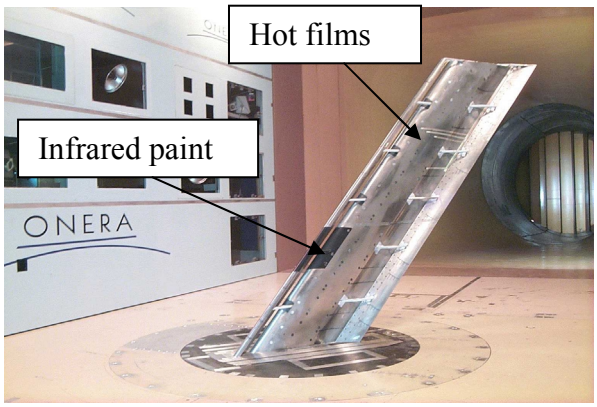

Figure 1 : AFV model into the F1 test section

Twenty four Dantec hot films were distributed on the 3 parts of the model (see fig. 2 : 9 on the slat, 9 on the wing and 6 on the flap). They were glued directly on the metallic wing and electrical connections were realised with thin copper strips.

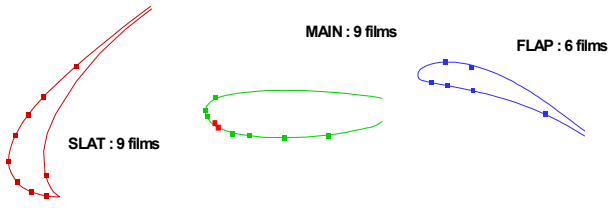

Figure 2 : Hot films locations on the AFV model elements (not at the same scale)

Two types of information were obtained from the hot films : RMS levels (measured during the polars and the stabilised points), and 1 second of signals stored in the stabilised phases. The chordwise evolution of the root-mean-square level (RMS of the output voltage of the hot films) indicates the state of the boundary layer and the transition location. The RMS level, particularly low in laminar flow, grows up, reaches a maximum in the intermittency region and comes down to the turbulent RMS level. The transition determination was done by the intersection between the nearly constant laminar level and the highest slope of the intermittency region growth ; this location corresponds to the beginning of transition.
We analysed also the signals evolutions and sometimes the skewness factor (third moment) to assess the transition location.

3 Numerical approach : tests preparation

In order to choose the right configurations for the tests and to optimise the transition determination devices, some pre-test computations have been performed. 3D Navier Stokes (RANS) computations were first done at ONERA (DAAP Department) in order to get the pressure distributions on the different elements, in the reference case : sweep angle 40° and flap set at 20°. Two angles of attack were considered to get a good idea of the L.E. contamination domain and to determine some transition locations (DMAE Department) and their evolution under the angle of attack and the Reynolds number effects.

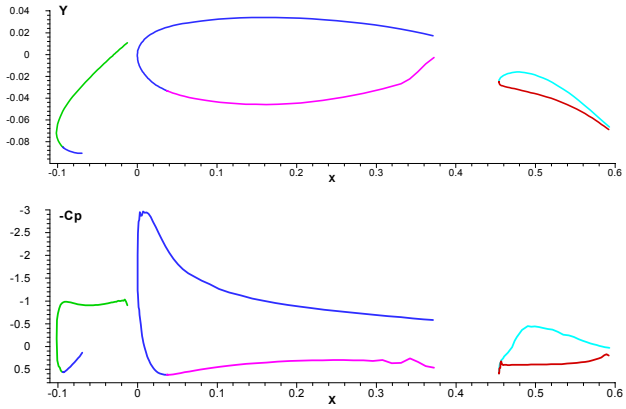

Figure 3 : Geometry and computed pressure distribution

The Navier Stokes results were obtained assuming a turbulent boundary layer and using a k-l turbulence model [2]. A multi–domain mesh was used for the 3D model and the data were given in a parallel to free stream coordinate system. Figure 3 shows the model geometry and the mid-span computed pressure distribution in a normal to leading edge direction.

Because the model is fixed directly on the wind tunnel floor, L.E. contamination is likely to occur for certain conditions. This problem has been analysed through the evolution of the Reynolds number : $\overline{R} = W_e \Big/ \sqrt{\nu \frac{\partial U_e}{\partial X}}$. From effective sweep angles, this parameter has been determined for the three elements, in order to help wind tunnel test preparation. According to an empirical criterion [3], L.E. contamination occurs for values above 250. $\overline{R}$ values show that the AFV model main wing will be contaminated in most wind tunnel conditions, at 40° sweep (fig. 4). Contamination is expected to appear on the slat at Re = 4.5 10^6. The flap should not be contaminated.

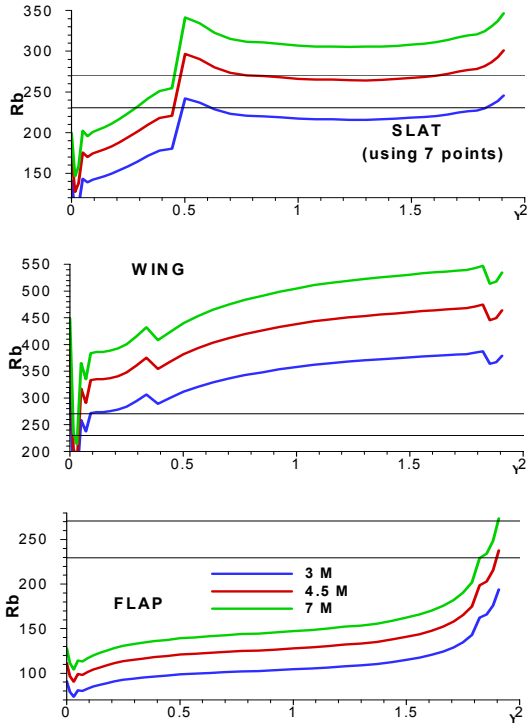

Figure 4 : Contamination of AFV elements at 40° sweep

In order to avoid main wing contamination, it was decided before the beginning of the tests to consider two values of the model sweep angle, 30 and 40°. The effective sweep angle variations are quite large along the model span, specially at the wing root. Infinite swept wing assumption should be acceptable 0.4 m above the wind tunnel floor and over a spanwise extend of about 1.3 m.

Preliminary transition prediction work was performed by FOI, DASA and ONERA on the AFV data [4]. Mid-span ONERA's transition predictions are presented in figure 5 taking into account L.E. contamination and using the simplified database method [5],[6]. As two separate models are used for longitudinal (TS) and crossflow (CF) instabilities, the envelope method is applied separately to these two instability types, and also in the classical way, covering TS and CF waves [7]. Thus three N factors are computed, the classical N_{env} for the envelope method, a N_{TS} for longitudinal waves and a N_{CF} for travelling crossflow waves. Transition is predicted assuming a constant N factor, equal to 7.15 for TS and CF waves.
At transition, the value of (N_{CF}, N_{TS}) closest to N_{env} gives an indication on the nature of transition, either CF or TS. In the presented cases, N_{TS} remains negligible in every cases, smaller than one. Boundary layer separation may also be predicted by the boundary layer code.

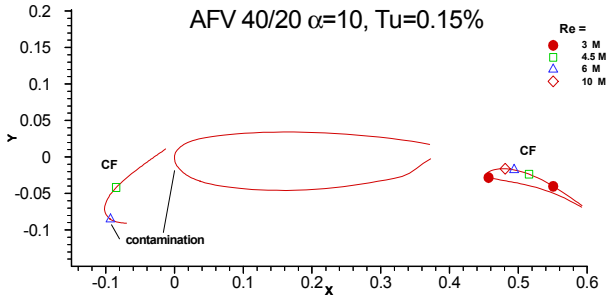

Figure 5 : Transition prediction on the 3 elements at 40° sweep

On the slat, boundary layer remains laminar for Re < 4.5 10^6. For Re = 4.5 10^6, transition moves upstream on the suction side, and for Re ≥ 6 10^6 L.E. contamination makes the leading edge turbulent. On the main wing, L.E.

contamination is always predicted for this configuration.
On the flap, separation is predicted on the pressure side very close to the attachment line, due to a small 'ripple' in the pressure distribution.

4 Typical results

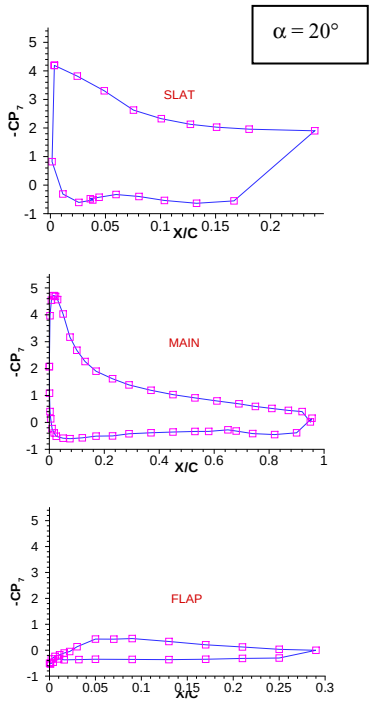

Figure 6 : measured Cp distributions φ = 40°, flap 20°

Three geometrical configurations have been tested (Sweep 40° / Flap 40°, Sweep 40°/ Flap 20° and Sweep 30°/Flap 20° with a fixed slat angle 30°), and for each model configuration, 6 aerodynamic conditions were investigated. All the cases have been analysed through the different model measurements :

- Cp distributions : typical pressure distributions measured on the 3 elements of the AFV model are presented in the reference configuration for α = 20° (fig. 6) We observed a good correlation with the pre-tests calculations.
- Hot film signals and RMS evolutions,
- Infrared images,
- L.E. contamination Reynolds number ; $\overline{R}$ computed from measured pressure are close to the pre-tests results.

In this paper we will not present all the results but instead illustrate the different types of transition which have been identified on this high lift generic model. The Reynolds numbers are based on the reference wing chord, not on the element dimension.

4.1 Leading edge contamination of the slat upper side :

This analysis has been performed for the three elements of the AFV model using hot films signals and with $\overline{R}$ computed using experimental Cp distributions.

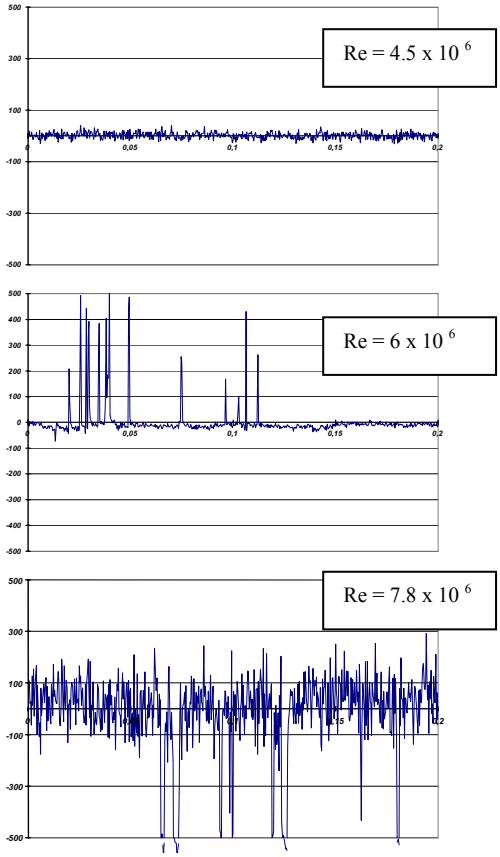

Figure 7 : Typical hot film time signals evolution α = 10°, φ = 40°, flap 40°

The first analysis of the tests results is relative to the contamination domain of the slat, using hot film signals. Figure 7 presents typical evolutions of hot films signals located around the slat leading edge (hot film 3) for 3 Reynolds numbers. In the first case (Re = 4.5 x 10^6) the signal remain absolutely laminar, in the last case (Re = 7.8 x 10^6) it is almost turbulent. Between these two there is a case (Re = 6 x 10^6) in

which some turbulent spots can be seen on the laminar signal, this case corresponds to the beginning of L.E. contamination. The signals analysis performed in other configurations allowed us to determine the experimental limit of attachment line transition.

The second analysis of the tests results is relative to the L.E. contamination of the slat using the $\overline{R}$ values .
$\overline{R}$ is plotted versus the angle of attack for different Reynolds numbers (fig. 8). When angle of attack is increasing, $\overline{R}$ values decrease first, before a stabilisation and a small increase in some cases for angles greater than 20°. This evolution is due to the leading edge radius change along the chordwise section when attachment line location changes with incidence. The radius is minimum close to X/C = 0 % and increasing in the upper or lower side directions. As expected, the shape of these curves seems to be independent of the Reynolds number Re, only the $\overline{R}$ levels are different.

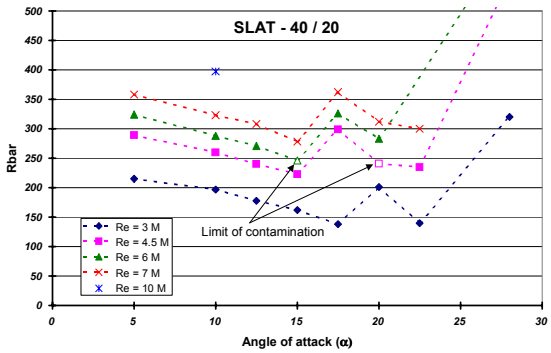

Figure 8 : Experimental $\overline{R}$ evolution φ = 40°, flap 20°

This analysis confirms the domain of L.E. contamination : the $\overline{R}$ values above 250 are relative to the configurations for which Re is greater than 6 x 10^6 and contamination process makes the slat boundary layer turbulent.
The same analysis confirms that the wing element is almost always contaminated and as we saw with pre-tests computations the flap is never in a contamination situation, as $\overline{R}$ values are always below 250.
Finally we can note that the experimental determination of the L.E. contamination (hot film) corresponds to $\overline{R}$ values rather close to 250, nevertheless the small number of hot films is not sufficient to determine accurately this limit.

4.2 Relaminarisation process :

During the analysis of the results we found only 3 cases in which the relaminarisation process might happen. To reach this phenomenon on the slat, two main conditions are needed. First the test Reynolds number must be higher than 6 x 10^6 in order to get turbulent conditions through the contamination process. Secondly the angle of attack of the model must be large enough to get a large acceleration around the leading edge. In these conditions the strong negative pressure gradient first damps the turbulent structures coming from the L.E. contamination and if the acceleration parameter is large enough the boundary layer can reach a local relaminarisation state as observed [8] on a 3D high lift configuration.

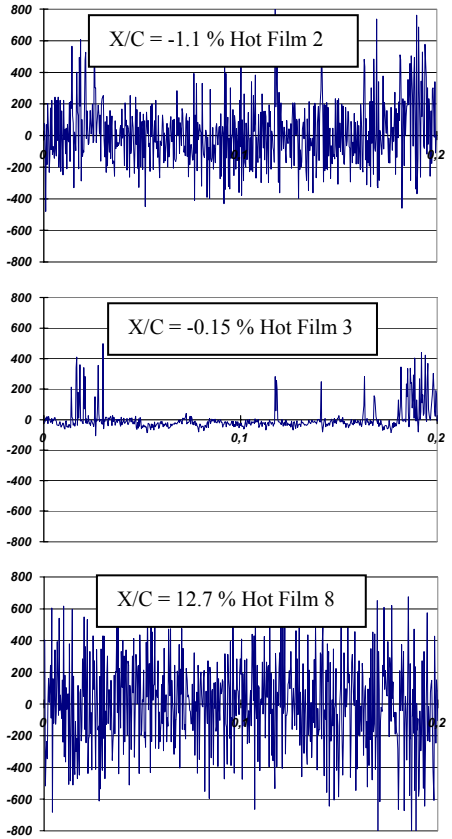

Figure 9 : Hot film time signal evolution on the slat upper side φ = 30°, flap 20°

The acceleration parameter defined by Beasley [9] :

$$K = \nu/U_e^2 * dU_e/dS$$

must be higher than 5 x 10^{-6} to reach a fully laminar boundary layer in 2D flow.
In our cases this parameter has been computed prior to the tests [4] in order to compare the present results to the previous one.

To verify experimentally the relaminarisation process, the hot film signals are plotted around the slat leading edge in the chosen case (fig. 9) and the skewness factor is calculated (fig. 10).
The signals are relative to the hot films (hf) hf2, hf3 and hf8 of the tested case : φ =30°, flap angle 20° at Re = 7.5 x 10^6 and α = 20°. This case is relative to a L.E. contamination case ($\overline{R}$ = 289). The acceleration parameter is between 3 x 10^{-6} and 4 x 10^{-6} and the attachment line is located between hf1 and hf2. As we can see in figure 9, hf2 is fully turbulent, hf3 looks like a laminar signal on which a few contamination turbulent spots are propagating. Further downstream hf5 has an intermittent signal and hf8 is fully turbulent.
To improve this analysis, we computed the skewness factor from the hot film signals. This parameter allowed to point out the intermittent regions of the slat upper side ; the skewness absolute value close to 0 in laminar and turbulent conditions grows above 0.5 for intermittent signals. This factor is plotted along the slat upper side (fig. 10) ; this evolution confirms relaminarisation around the slat leading edge.

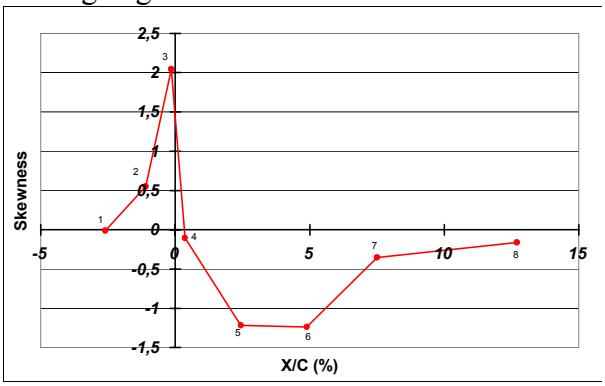

Figure 10 : Typical relaminarisation case φ = 30°, flap 20°

Nevertheless, in our configuration the value of the acceleration parameter, located just under the Beasly criterion, perhaps doesn't allow to reach a complete relaminarisation.
Finally, on this high lift study, we found a relaminarisation (partial) only on the slat upper side for Reynolds numbers greater than 6 x 10^6 and high angles of attack.

4.3 Transition in a separation bubble :

The infrared visualisations allow to note the limit between the clear laminar part (close to the leading edge) and downstream, the dark turbulent one. At high angle of attack we can see a well defined line connected to the presence of a separation bubble ; in such cases the line doesn't represent the transition line, but it corresponds to the end of the laminar (or transitional) separation bubble.
When the angle of attack increases for a given aerodynamic condition, the transition location moves upstream on the slat.

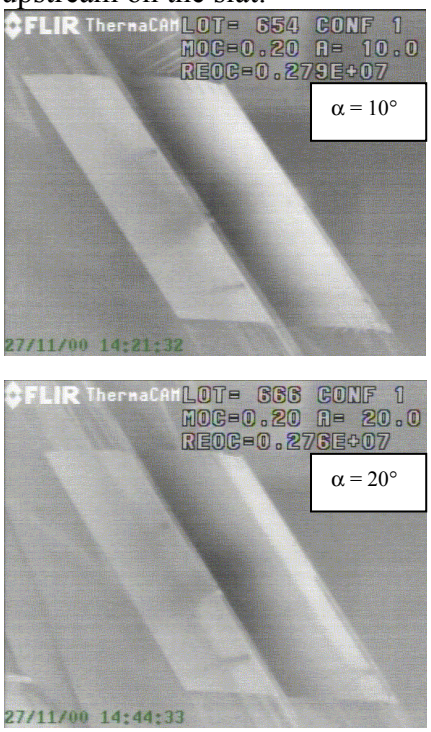

Fig. 11 : Typical infrared images case φ = 40°, flap 20°

At low angle (see fig. 11 upper part) on the infrared image there is a free 3D transition on the slat upper side. When angle of attack is increasing, we can observe a laminar bubble

which appears for angles greater than 15° at low Reynolds numbers (see fig. 11 lower part). In the reference configuration (φ = 40°, flap angle 20°) the natural transition was forced by the separation bubble for angles of attack from 20° and Re less than 6 x 10^6.
In fact the separation bubble is connected to the positive pressure gradient located, on the slat upper side, just downstream of the suction peak, close to the leading edge, on the Cp distributions. This peak becomes large when angles of attack are increasing.
In the cases of high Reynolds numbers, the separation bubble was not visible on the infrared images according to the limit of L.E. contamination.

4.4 Natural transition analysis :

- *transition with streamwise instabilities*

We first remind the Cp distribution on the slat upper side (fig. 12) in order to see that the flow is decelerated from about X/C = 2.5 %. In these conditions, for low angles of attack (less than 15°) and low Reynolds numbers (to avoid L.E. contamination) when transition is located in the positive pressure gradient, Tollmien-Schlichting are dominant instabilities developing in the boundary layer.

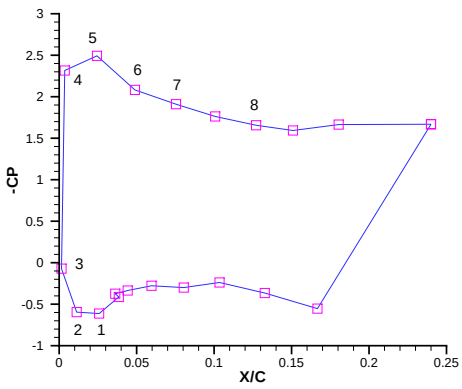

Figure 12 : Cp distributions on the slat upper side φ = 40°, flap 20° and α = 15°

The transition evolution on the slat upper side has been determined mainly with the hot films information (RMS levels and hot film signals) completed by the infrared images.

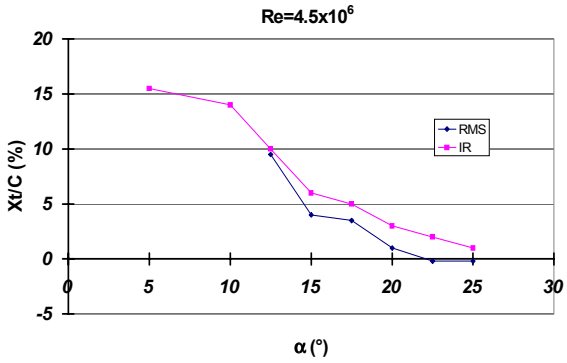

Figure 13 : Comparison between RMS and infrared determinations φ = 40°, flap 40°

A comparison of RMS and infrared transition location determinations is given for the same geometric configuration at Re = 4.5 x 10^6. Generally the infrared images gives the middle of the transition location while our RMS analysis provides the beginning of transition. In this high lift configuration we can observe an increasing gap between these 2 determinations when angle of attack is increasing (fig. 13), probably due to the presence of a laminar separation bubble for high angles of attack (more than 15°). In such cases the infrared image gives the end of the separation bubble, not the transition location.
All the tested configurations have been analysed in terms of transition location determination on the slat upper side and the results are plotted in figure 14. The drawing summarises quite properly the laminar domain of the slat upper side as a function of the Reynolds number and the angle of attack.

Finally for angles of attack over 15° - 17.5°, there is a laminar bubble separation and transition is almost independent of the Reynolds number (see fig. 14). Concerning the high Reynolds numbers (more than Re = 6 x 10^6), we can remind that the slat upper side is contaminated.

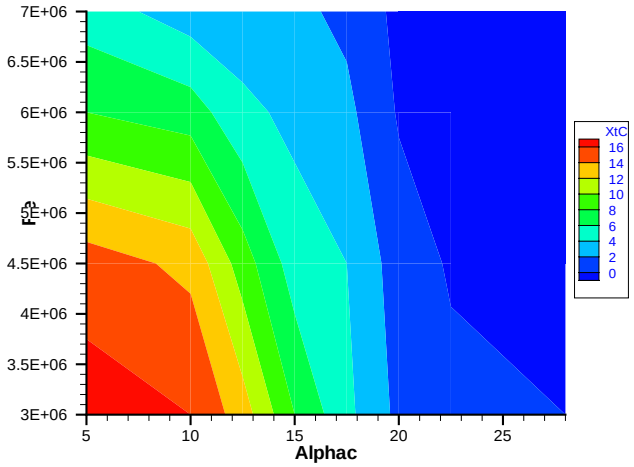

Figure 14 : Laminar domain of the slat upper side

- *transition with crossflow instabilities*

The wing element is almost always contaminated. At low angles of attack (α = 5° and 10°) and low Reynolds number there is a small laminar region on the wing lower side at low sweep angle. On the Cp distribution (fig. 15) there is a negative pressure gradient from X/C = 6% up to 45 %. If the transition is located in the accelerated part of the pressure lower side, we can think that crossflow instabilities are amplified in the boundary layer.

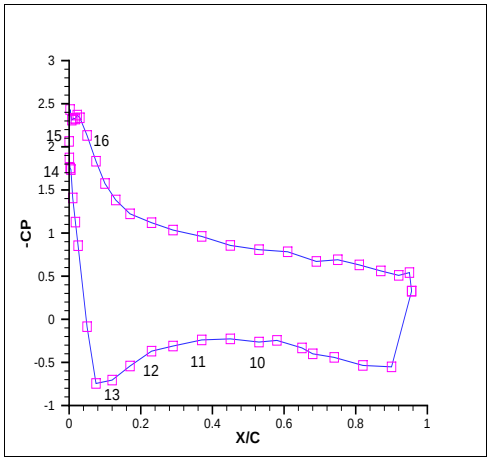

Figure 15 : Cp distributions on the wing lower side φ = 30°, flap 20° and α = 5°

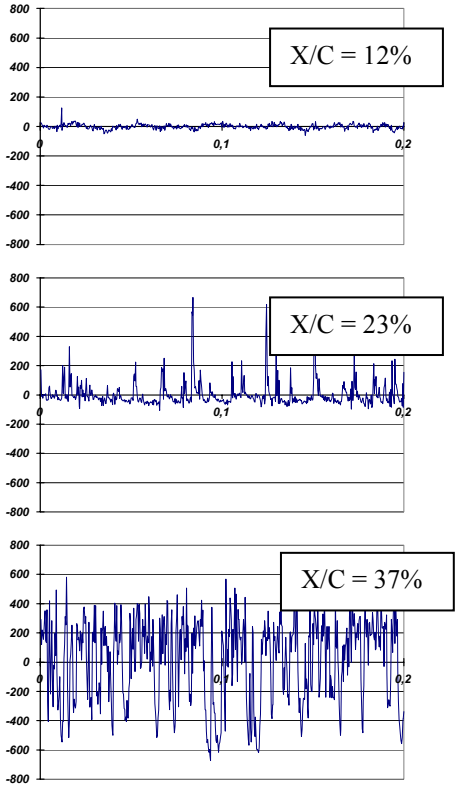

Figure 16 : Hot film time signal evolution on the wing lower side φ = 30°, flap 20°, α = 5°

Hot films are located in the accelerated part of the wing lower side. The signals evolution shows a transition located close to X/C = 40 % in the negative pressure gradient (fig. 16). The transition may occur under crossflow instabilities which are developing in the accelerated region of the wing lower side.
The TS/CF classification has to be confirmed by computations, as transition may appear in a low pressure gradient region (TS) after a region of strong negative pressure gradient associated to CF waves.

5 Conclusion

In order to study the effect of Reynolds number on the transition location in high lift case, a basic study has been carried out in the framework of the EUROLIFT programme using the AFV swept wing model. The tests have been performed at different sweep angles and different Reynolds numbers, in the F1 low speed pressurised wind tunnel located at the ONERA centre of 'Le Fauga Mauzac'.

This existing metallic model is well equipped with pressure taps (744) and we added an area of observation for the infrared camera on the slat upper side and 24 hot films distributed on the slat, the wing and the flap in order to determine the transition location.
In the preparation phase of the tests, N.S. computations have been performed in order to get transition predictions using the simplified data base method. This numerical approach has been performed in one configuration and the prediction are in good agreement with the experimental results. Moreover attachment line transition Reynolds number was computed and the predicted results are close to those analysed with the experimental Cp distributions.

So on the slat element we observed a transition evolution connected to the angle of attack and Reynolds number effects. We measured different transition mechanisms such as free transition including transition forced by a separation bubble or L.E. contamination. Finally we observed only one configuration for which relaminarisation process was observed.
Concerning the free transition cases, the numerical approach of the EUROLIFT task 2.3 will clarify the TS and the CF transitions.
The wing element is almost always contaminated. At low angles of attack, low sweep angle and low Reynolds number we observed a laminar region on the wing lower side.
The flap element is never contaminated.

Acknowledgements :

The EUROLIFT research project has been co-financed by the 5th Research Framework Programme of the European Union (EU).

References

[1] D. Cassoudesalle
EUROLIFT tests in F1 wind tunnel.
Test report : PV 71/0534 DAAP/DSFM – January 2001

[2] S. Ben Kheli, J.L. Gervois, G. Carrier, F. Moens, P. Viscat
Assessment of elsA software through civil transport aircraft configurations.
CEAS Aerospace Aerodynamics Research Conference, Cambridge, UK, June 2002

[3] D. I. A. Poll
Some aspects of the flow near a swept attachment line with particular reference to boundary layer transition.
Cranfield Institute of Technoloy, CoA Report N°7805 (1978)

[4] J. Perraud
Transition prediction for high lift applications.
Implementation of database method in boundary layer codes and preliminary validation.
EUROLIFT Final Report TR2.3-1 – January 2001

[5] D. Arnal
Transition prediction in transonic flows
Zierep and Oertel Editors. Transsonicum III. IUTAM Symposium, Göttingen – 1988

[6] G. Casalis, D. Arnal
Database method – Development and validation of the simplified method for pure crossflow instability at low speed
ELFIN II Subtask 2.3 - ELFIN II Tech. Rep. N° 145, 1996

[7] G. Schrauf, J. Perraud, D. Vitiello, F. Lam
Comparison of boundary layer transition. Predictions using Flight Test Data.
Journal of Aircraft, Vol. 35, N°6, 1998

[8] D. Arnal, J. C. Juillen
Leading edge contamination and relaminarisation on a swept wing at incidence.
Fourth Symposium on numerical and physical aspects of aerodynamics flows, California State University – Long Beach, 1989

[9] J.A. Beasley
Calculation of the laminar boundary layer and prediction of transition on a sheared wing. RAE Farnborough, Report N° 3787, 1976.